Nanoscale

COMMUNICATION

Molecular Conformations of DNA Targets Captured by Model Nanoarrays

Received 00th January 20xx,
Accepted 00th January 20xx

DOI: 10.1039/x0xx00000x

www.rsc.org/

X. Hao,[a] E. A. Josephs,[b] Q. Gu,[b] and T. Ye*[a]

An open question in single molecule nanoarrays is how the chemical and morphological heterogeneities of the solid support affect the properties of the biomacromolecules. We generated arrays that allowed individually-resolvable DNA molecules to interact with tailored surface heterogeneities and revealed how molecular conformations are impacted by surface interactions.

An emerging need in single molecule measurement is to arrange individual biopolymer molecules in an array format[1] to improve the throughput of measurement in a host of applications, such as single molecule biophysics,[2] single molecule sequencing[3] and epigenetic analysis.[4] An open question is how the interactions between DNA and the solid support of the array impact the conformations, molecular recognition, and other biophysical phenomena of the DNA molecules, which are intimately linked to the device performance.[5] Even a carefully prepared surface could have anomalously strong adsorption sites that significantly impact the dynamics of macromolecular adsorbates.[6] Therefore, patterned surfaces, which have compositional heterogeneities (non-uniform lateral distributions of surface functionalities and probe molecules)[7] as well as morphological heterogeneities (surface roughness),[8] may have unexpected and pronounced effects on these molecular properties. Such heterogeneities have been recognized as a contributing factor to the limited reproducibility of many DNA microarrays[5,9] and could have an even more pronounced impact on single-molecule nanoarrays. [1, 4, 8, 10]

There exist two major barriers toward a fundamental understanding of the molecular properties of DNA on nanoscale surface patterns. First, because the relevant length scales of surface interactions are typically less than a few nanometers,[11] to understand how surface patterns interact with DNA, the morphological and compositional heterogeneities need to be controlled at the relevant spatial scales. Common patterning techniques[12] lack the ability to define the morphology and the lateral distribution of surface chemical functionalities with this level of precision, and hence the resulting arrays may be too complex for fundamental investigations.[5] Second, common characterization techniques, such as surface plasmon resonance,[13] X-ray photoelectron spectroscopy,[7] electrochemical techniques,[14] while capable of detecting the amount of targets/probes, have neither the spatial resolution nor the specificity to directly probe nanometer-scale interactions or their effects on microscopic processes such as adsorption, desorption, diffusion, and molecular recognition.[15] Single-molecule fluorescence microscopy studies revealed that functionalized surfaces have isolated nanoscale sites that can mediate unfolding of biopolymers, despite the low surface coverage.[6] However, the exact origin of such nanoscale anomalous sites is difficult to elucidate even with super-resolution localization, as fluorescent labeling of such sites is typically impracticable and the spatial resolution (~20-50 nm) remains insufficient. We seek to understand the roles of surface heterogeneities in DNA layer end tethered to self-assembled monolayers (SAMs) on gold (**Figure 1**),[16] which have broad utility in DNA sensors and micro/nanoarrays.[14, 17] Recent studies suggest that the surface heterogeneities in the DNA monolayers, such as non-uniform probe densities, may impact the sensitivity and reproducibility of these DNA biosensors and arrays.[18] In this study, we have conducted high resolution, label-free, single molecule AFM imaging of DNA molecules captured by a model nanoarray with precisely introduced compositional as well as morphological heterogeneities. We produced array patterns of ordered SAMs with a lateral dimension as small as ten nanometers, an edge width of only a few nanometers or less, and topographical height controlled with angstrom-level precision, as well as spatially resolved single DNA probe molecules.[10, 19] These single molecule patterns were made by using the AFM tip to displace thiol molecules in a preformed SAM under a mixture solution of these thiolated probe molecules with spacer thiol molecules that can compete for binding to the exposed Au surface(see Figure 1).[10] These probe molecules can capture larger DNA targets and place them in close proximity to the nanoengineered surface feature.

[a] *School of Natural Sciences, University of California, Merced, California, USA*
Email: tao.ye@ucmerced.edu
[b] *School of Engineering, University of California, Merced, California, USA*
† Footnotes relating to the title and/or authors should appear here.
Electronic Supplementary Information (ESI) available: [Methods and additional data]. See DOI: 10.1039/x0xx00000x

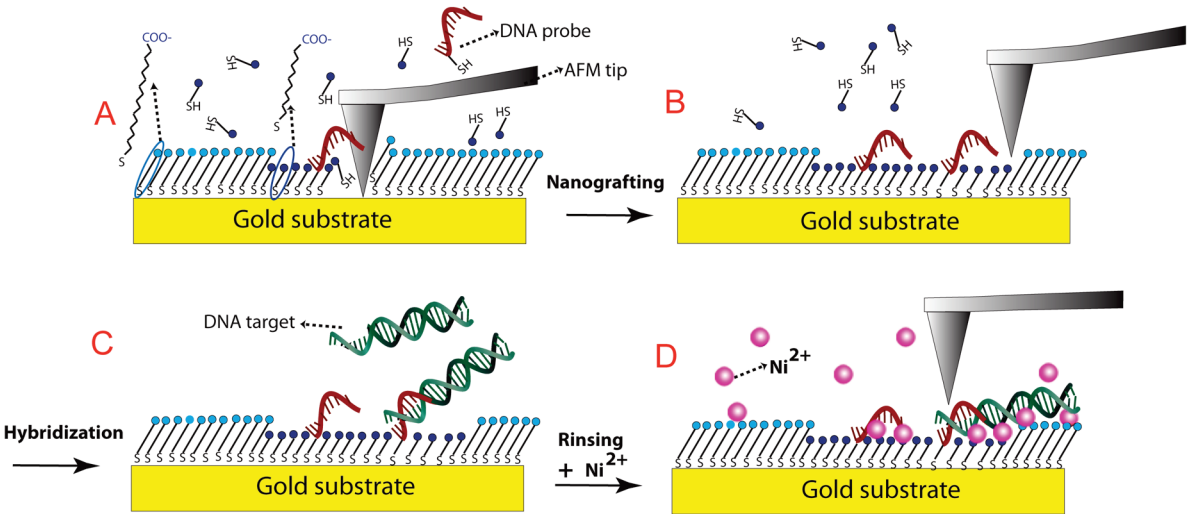

Fig. 1 Schematic illustration of nanografting surface chemical patterns with DNA probes and capture of DNA targets. (A) A large force was applied on the AFM tip to displace the thiol molecules in the MHDA SAM on an Au(111) substrate. (B) The thiol molecules in the solution, 24 nt ssDNA with -$C_{11}H_{22}SH$ tethers and MUDA form a mixed monolayer on the exposed gold surface. (C) The ssDNA molecules (DNA probes) can capture double-stranded DNA with a single-stranded segment. Hybridization was carried out in a monovalent cation buffer. (D) The addition of a divalent cation, such as Ni^{2+}, can immobilize the DNA and allow high resolution, single molecule AFM imaging.

Moreover, to address the challenge that the mobility of the DNA molecules on these SAM surfaces preclude high resolution AFM imaging in a buffer solution,[17, 20] we have used carboxyl terminated SAMs that can dynamically switch interactions with DNA: in the absence of divalent cations, the anchored DNA molecules are lifted up from the negatively charged surface and free to interact with other biomolecules in the solution; in the presence of divalent cations, the DNA probe and target molecules are pinned down to the surface, allowing us to visualize the spatial distribution of molecules and how DNA molecules interact with the surface patterns.[21] The label free, nm resolution single molecule imaging revealed that the conformation of surface-tethered DNA may be highly sensitive to the compositional and morphological heterogeneities of the surrounding chemical pattern: the DNA target molecules were found to preferentially adhere to the boundary between two carboxyl terminated monolayer domains that differ by only half a nanometer in topographical height. The study raises new questions on how target-capture in an array may be impacted by such surface heterogeneities. Moreover, we demonstrate that these nanoscale interactions can be exploited to control the conformation of DNA molecules and align the molecules into novel shapes. The ability to selectively capture long DNA in spatially addressable arrays and achieve control over the molecular conformations may enable new applications in single molecule measurement. In addition, understanding and controlling the interactions between DNA and surface patterns at the single molecule level can facilitate the self-assembly of complex DNA nanostructures on solid surfaces.[22] We performed nanografting in a solution containing 24 nucleotide (nt.) single-stranded DNA (ssDNA) molecules that each possessed a –C11H22SH tether, and 11-Mercaptoundecanoic acid (MUDA) spacer molecules into a pre-assembled host SAM composed of 16-Mercaptohexadecanoic acid (MHDA) (Figure 1A, B). AFM images showed that after nanografting, depressed areas that are 0.5±0.1 nm deep appeared (Figure 2 and Figure S2). These depressions correspond to MUDA SAM, which is approximately 0.6 nm thinner than the host MHDA SAM. In the presence of Ni^{2+}, protrusions that are 0.7 ± 0.2 nm taller (see histogram in Figure S3) than the depressed regions are also observed (arrows in Figure 2A). These protrusions correspond to patterned ssDNA probe molecules that have the thiol tether anchored to the gold surface and the DNA segment pinned atop the COOH terminated monolayer (Figure 1).[21, 23] Then we exposed the surface pattern to a 1x Tris acetate EDTA (TAE, 40 mM Tris, 20 mM acetic acid, and 1 mM EDTA) buffer containing 100 nM of DNA "target" molecules for 30-60 min (Figure 1C). Each of the target molecules has a 372 bp double-stranded DNA (dsDNA) segment and a 24 nt. single-stranded segment that is complementary to the probe DNA (Supporting Information). After the surface was rinsed with a TAE buffer, it was imaged under an imaging buffer that contained 5 mM Ni^{2+} and 4 mM Tris acetate (Figure 1D). The AFM measurement (Figure 2B) shows rod-like features that are 120 ± 20 nm long and 2.0 nm high (over 100 molecules were analyzed). As we have demonstrated in previous studies,[21, 24] these features correspond to dsDNA molecules immobilized onto the SAM surface. In a control experiment where a nanografted pattern that is free of DNA capture probes was exposed to the same DNA target solution, no features of DNA targets were observed on the surface (Figure S4). The results confirm that the patterned DNA probes can capture the target DNA through base-pairing interactions.

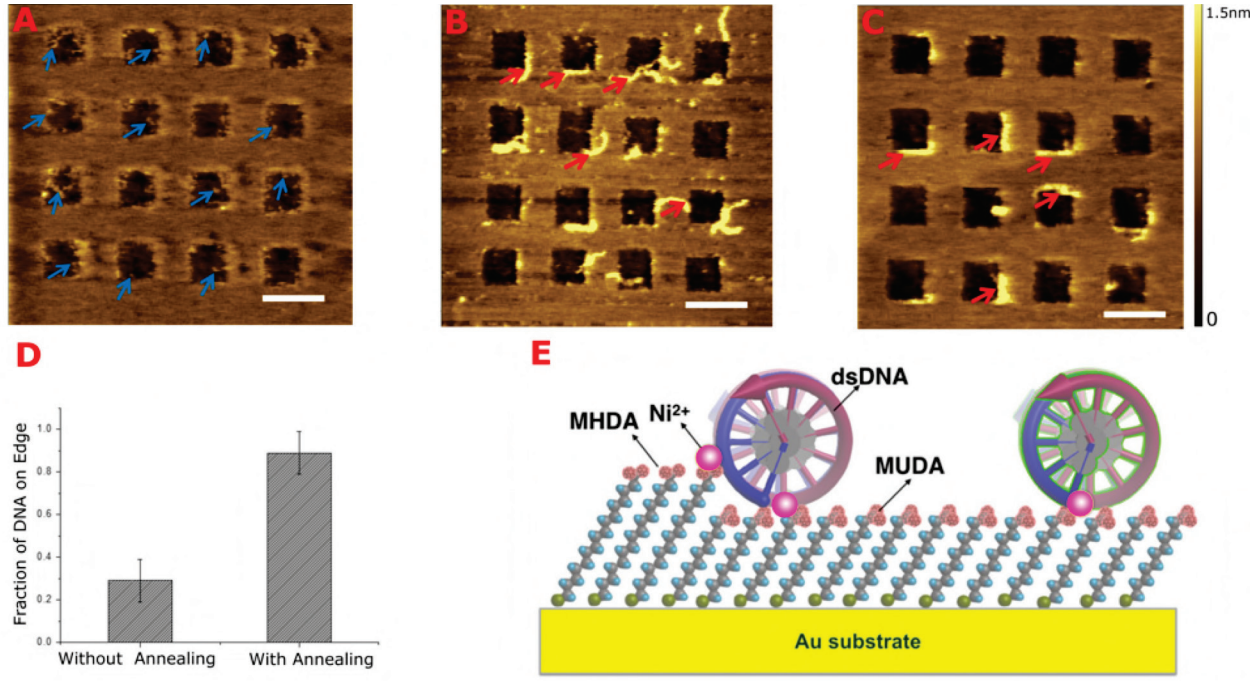

Fig. 2 (A) AFM topographical image of nanografted DNA pattern before target capture. The squares are nanografted features containing MUDA and ssDNA probes (protrusions marked by blue arrows). (B) AFM image of an array that was exposed to dsDNA targets. Images were acquired under 5 mM Ni^{2+} in a 0.1X TAE buffer solution by tapping mode AFM. Red arrows mark some of the features corresponding to captured targets. (C) AFM image of captured DNA targets that were immobilized using an annealing procedure: 1 mM Mg(II) was added to the TAE buffer every 2 min, up to 10 mM Mg(II) in total. The nanoarray was then transferred to an imaging buffer (5 mM Ni(II) buffer). The scale bar is 200 nm. (D) The fractional length of DNA adhering to MUDA/MHDA boundaries without and with the annealing step, the error bar is the standard deviation of the average fractional lengths of 8 separate AFM images containing ca.120 dsDNA molecules. (E) Schematic showing possible interactions between DNA and a MUDA/MHDA domain boundary. The stronger adhesion to the edge is hypothesized to originate from additional salt bridging interactions at the top of the edge.

Interestingly, a number of the DNA molecules were aligned along the edges of the squares (Figure 2B). The preferential adhesion to the boundaries between MUDA and MHDA SAMs, which have the same surface groups but differ by ~0.6 nm in topographical height (Figure S2), indicates the impact of morphological heterogeneity. However, the degree of the preference is likely affected by kinetic trapping of DNA caused by strong surface immobilization in the presence of Ni^{2+}.[25] To evaluate if the edge sites are indeed the energetically preferred sites for DNA, we adopted an "annealing" protocol that gradually increases the strength of the surface interactions to allow the DNA molecules to explore the different binding sites and settle into low energy configurations. The strength of the surface interactions was tuned by adjusting the buffer composition: in a monovalent buffer, the end-tethered DNA molecules interact only weakly with the surface because both the DNA and the surface are negatively charged;[21] divalent cations induce attractive interactions between the DNA molecules and the carboxyl terminated surface.[21] In a separate study (in preparation), we also discovered that the interactions between DNA and the carboxyl surfaces are notably weaker in Mg^{2+} than those in Ni^{2+}, a trend that was also observed for DNA adsorbed on mica surfaces.[26] Therefore, to gradually increase the binding strength, we first added 1 mM Mg(II) to the TAE buffer every 2 minutes, up to 10 mM Mg(II) in total, and then transferred the surface to an imaging buffer that contained 5 mM Ni^{2+}. The fraction of the DNA contour length that adheres to the edge increased dramatically, from 29% to 89% (Figure 2C). The preferential binding is remarkable considering that it is not possible for many DNA targets to fully align with the edges as many of the DNA probes are located away from the edges. In addition, the straight conformation is a sharp departure from the semi-flexible worm-like chain conformation that is observed in the solution phase as well as on unpatterned surfaces.[24, 25] The results confirm that compared to flat surfaces, DNA molecules near the edge are stabilized by strong interactions.

The origin of the stronger attractive interactions at MUDA/MHDA boundaries in the presence of divalent cations is an open question. The attractive interactions between DNA and a flat carboxyl terminated SAM are thought to be induced by divalent cations that bridge between the two negatively charged objects. Such salt bridging interactions may originate from electrostatic (counterion-correlation) [27] or chemical forces (the metal ions likely form coordination bonds with both the phosphate backbone of the DNA

and the carboxylate groups on the surface). Regardless of the origin, the divalent cations must be within less than a few angstroms away from the functional groups for such attractive interactions to occur. The short length scale of these interactions explains why the attractive interactions at MUDA/MHDA boundaries are stronger than those on a flat carboxyl surface: due to the curvature of DNA, additional divalent cations can bridge DNA and the carboxylate groups at the top of the edge, increasing the interactions between DNA and the MUDA/MHDA domain boundary (Figure 2E).

Another possible origin for the preferential binding at the MUDA/MHDA is the partial exposure of the hydrophobic alkyl chains of MHDA, as MHDA is 5 methylene groups longer than MUDA. Hydrophobic surfaces are known to favour the adsorption of DNA.[28] To test if hydrophobic interactions at the edge alone are responsible for the preferential binding of DNA, we used a host SAM of 16-Mercaptohexadecanol (MHD), which has an identical hydrocarbon chain and a hydroxyl terminal group that does not strongly interact with divalent cations (**Figure 3**). An AFM image of the pattern revealed DNA probe features as well as depressed

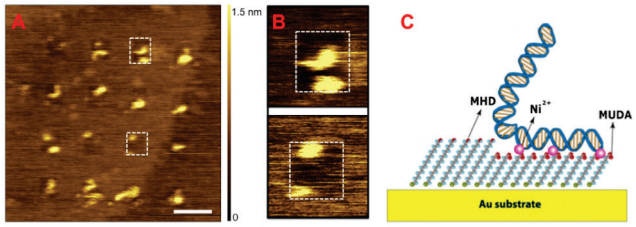

Fig. 3 (A) AFM image of dsDNA targets captured by a nanoarray of MUDA in a host SAM of Mercaptohexadecanol (MHD), $HS(CH_2)_{16}OH$. The protrusions, which are 2 nm high, correspond to double-stranded DNA molecules. (B) Zoom in images of nanografted areas in (A). The dotted squares are used to outline the nanografted squares. (C) Schematic of DNA interacting with nanografted boundary of MUDA and MHD. The dsDNA target was immobilized by Ni^{2+} on MUDA. However, because Ni^{2+} cannot bind to MHD, the segment that is over MHD is not immobilized and hence is not imaged by AFM. Scale bar is 200 nm.

MUDA squares that are 0.3 nm deep (Figure S5), which is smaller than the physical height difference between the MUDA and MHD SAMs, ~0.6 nm. The smaller topographical contrast is attributed to the difference in how the two SAMs interact with the AFM tip, which is terminated with a negatively charged SiO_2 layer. Compared to the neutral MHD SAM, the negatively charged MUDA SAM has a stronger repulsive interaction with the AFM tip. The AFM image of the surface after exposure to dsDNA target molecules showed protrusions that are 1.8 nm $\pm$ 0.2 nm high and 50 nm $\pm$ 20 nm long (see histogram in Figure S6) in the nanografted MUDA regions. These protrusions are too high and too long to be single-stranded DNA probes on MUDA (see Figure 2A and ref. [21]). Instead, the height corresponds to that of a dsDNA target as shown in previous studies.[21, 24] In contrast with Figure 2C, the molecular features in Figure 3A and Figure 3B have no strong preference to adhere to the MUDA/MHD boundaries. Moreover, unlike those in Figure 2B and C, the lengths of the features are significantly below the full contour length, 131 nm. Similar partial features of dsDNA were observed in previous AFM studies[29] and indicate only a part of the molecule is pinned to the surface and the rest is too mobile to be imaged (Figure 3C). Hydroxyl terminated SAMs do not immobilize DNA at the open circuit potential[29] and the 100 nm × 100 nm MUDA squares may be too small to immobilize the entire length of a target DNA, one end of which that is hybridized with a DNA probe molecule inside a square (Figure 3C). Overall, the results show that the hydrophobic interactions at the MUDA/MHD boundaries alone are not sufficient to immobilize DNA. Hence, carboxyl groups at the top of the edge are responsible for the preferential binding of DNA to MUDA/MHDA boundaries (Figure 2C). DNA that are adsorbed to the bottom of the edge, i.e., at the side of MUDA, may be stabilized by additional salt bridging interactions with carboxyl groups at the top of the edge. In addition, some of the DNA molecules are also adsorbed at the top sides of the edge, i.e., at the side of MHDA (Figure 2B). This suggests that the carboxyl groups of MHDA near the edge have a stronger affinity with DNA than COOH groups on a flat SAM surface. It is known that COOH SAMs have a higher pKa than free molecules in the solution, due to electrostatic repulsion between the ionized groups as well as tendency to hydrogen bond with neighbouring COOH groups.[30] The longer chain MHDA molecules near the edge may be more disordered due to greater exposure to water. Hence, compared to the COOH terminated molecules on flat surfaces, the COOH groups at the top are less likely to hydrogen bond with neighbouring groups and more likely to be in the ionized form that is responsible for salt bridging interactions with DNA.

In the development of single molecule nanoarrays, the DNA molecules need to be not only patterned in a spatially addressable manner but also stretched and aligned to localize specific sequences,[31] DNA binding proteins[32] or epigenetic markers[4] along the length. Fluid flow-based methods[2, 35] can align DNA along only a single direction. We hypothesized that strong binding of DNA along the edges of MUDA/MHDA patterns may be utilized to orient DNA molecules. We nanografted parallel long stripes of MUDA and ssDNA probe molecules into a host MHDA SAM matrix. Then we exposed the surface to a buffer containing the DNA target and used the aforementioned annealing procedure to progressively increase the interaction between the DNA and the surface. The AFM images showed channels that are 50 nm wide and 0.7 nm deep, as well as chains that are 1.1 nm higher than the MHDA regions, *i.e.,* 1.8 nm higher than the MUDA regions (**Figure 4**A. See also Figure S6A for patterned channels imaged prior to hybridization with the target dsDNA). These features resemble those in Figure 2C, and indicate that DNA adhere to the patterns in a manner dictated by the geometry of the nanografted shapes. In a separate experiment, we incubated the nanografted MUDA/ssDNA patterns with longer DNA targets (1000 bps) containing a short, complementary ssDNA tail (Figure S6B). The results also indicated a clear preference for the DNA to be parallel to the edges.

Next, we explored if the MUDA/MHDA boundaries can be used to align DNA along arbitrary directions on the surface by creating hollow squares and triangles of ssDNA probes and MUDA within a host MHDA SAM (Figure 4C and 4D). The AFM image showed chains

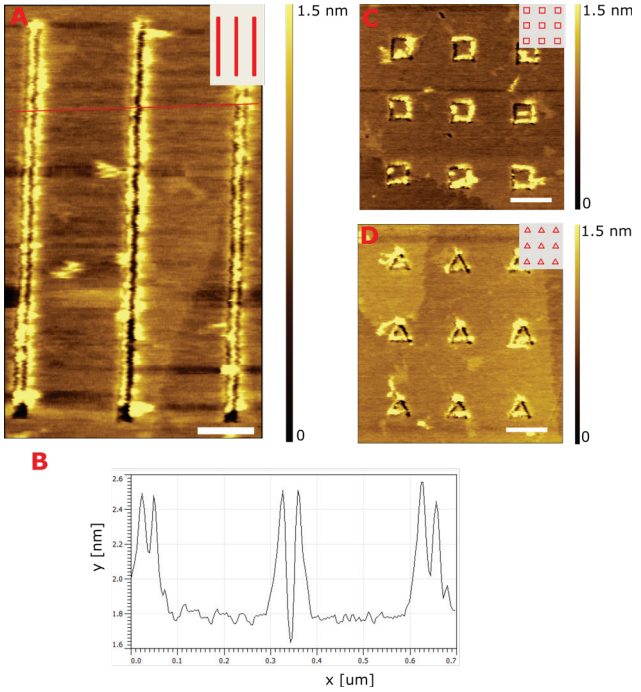

Figure 4. AFM images of dsDNA targets aligned with MUDA/MHDA boundaries. Images were acquired under 5mM Ni(II) in a 0.1x TAE buffer solution. Insets are the designs of surface patterns. Red features represent areas of MUDA and grey areas represent the host MHDA SAM. (A) DNA adhering to parallel gaps. (B) Corresponding cross-sectional profile. The heights suggest that the DNA protrudes ~ 2nm above the MUDA region. (C) DNA adhering to rectangular frames. (D) DNA adhering to triangular frames. The scale bar is 200 nm. Insets are the designs of the surface patterns.

that are 1.5 nm higher than MHDA regions and 2.0 nm higher than MUDA regions. Indeed, many of the DNA molecules align along the edges of the square and triangular shapes. It should be noted that some of the target DNA molecules appear to be crowded out of the pattern and are instead deposited on the MHDA SAM, possibly due to a higher density of DNA probes. Although further work optimizing nanografting and annealing conditions would be needed for more effective molecular alignment, the results here clearly indicate the potential of using surface chemical patterns to align DNA molecules into arbitrary nanoscale conformations.

Conclusions

Single molecule, high resolution imaging of model nanoarrays has revealed surprising effects of nanoscale surface chemical functionality and morphology on the molecular behaviors of DNA. We are currently quantifying the interaction forces between DNA and these SAMs with single molecule force spectroscopy. Future studies that investigate how such interactions impact the kinetics of DNA hybridization may help optimize molecular recognition in microarrays/nanoarrays. On a practical level, our approach combines the ability to orient long DNA molecules with a spatially addressable array format. DNA targets may be site-specifically captured using patterned oligonucleotides, and elaborate control over the shape and orientation of DNA molecules can be achieved with the chemical patterns. In addition to enabling nanoarray measurements, the knowledge in how DNA interact with surface chemical patterns on a solid support could also aid the development of novel complex DNA architectures on surfaces. Although patterning complex DNA structures on a solid support has attracted notable interest because of potential applications in nanophotonics, nanoelectronics, and nanoarray detection, existing efforts to assemble complex DNA structures on a solid support have been hindered by the limited control over the interaction between DNA and the surface.[22, 34] *E.g.*, the compositional heterogeneity of the mica substrate used for those studies was found to be responsible for low reproducibility in surface assembled structures.[22] Our approach may help advance the self-assembly of DNA on surfaces by enabling precise surface patterns that have more predictable and tunable interactions with DNA. Our approach to overcoming kinetic traps through dynamically adjusting DNA-surface interactions may serve as a general strategy that can reduce defect formation in self-assembly of complex DNA structures on surfaces.

Acknowledgements

The authors acknowledge the support of National Science Foundation, NASA (NNX15AQ01A), and University of California Cancer Research Coordinating Committee.

Notes and references

1 S. Howorka and J. Hesse, *Soft Matter* 2014, **7**, 931.
2 T. Fazio, M. L. Visnapuu, S. Wind and E. C. Greene, *Langmuir* 2008, **18**, 10524.
3 R. Drmanac, A. B. Sparks, M. J. Callow, A. L. Halpern, N. L. Burns, B. G. Kermani, *et al. Science* 2010, **5961**, 78.
4 A. Cerf, H. C. Tian and H. G. Craighead, *ACS Nano* 2012, **9**, 7928; M. Levy-Sakin, A. Grunwald, S. Kim, N. R. Gassman, A. Gottfried, J. Antelman, *et al. ACS Nano* 2014, **1**, 14.
5 A. N. Rao and D. W. Grainger, Biomater. *Sci.* 2014, **4**, 436.
6 M. J. Wirth and D. J. Swinton, *Anal. Chem.* 1998, **24**, 5264; J. S. Weltz, D. K. Schwartz and J. L. Kaar, *ACS Nano* 2015, **1**, 730; B. B. Langdon, R. B. Mirhossaini, J. N. Mabry, I. Sriram, A. Lajmi, Y. Zhang, *et al. ACS Appl. Mater. Int.* 2015, **6**, 3607.
7 A. N. Rao, N. Vandencasteele, L. J. Gamble and D. W. Grainger, *Anal. Chem.* 2012, **24**, 10628; N. Nelson and D. K. Schwartz, *Langmuir* 2015, **22**, 6099.
8 M. Palma, J. J. Abramson, A. A. Gorodetsky, E. Penzo, R. L. Gonzalez, M. P. Sheetz, *et al. J. Am. Chem. Soc.* 2011, **20**, 7656.
9 A. Sassolas, B. D. Leca-Bouvier and L. J. Blum, *Chem. Rev.* 2008, **1**, 109.
10 E. A. Josephs and T. Ye, *J. Am. Chem. Soc*. 2010, **30**, 10236.
11 J. N. Israelachvili, *Intermolecular and surface forces*, Academic Press, San Diego, USA 2015.
12 D. Qin, Y. Xia and G. M. Whitesides, *Nat. Prot.* 2010, **3**, 491; K. Salaita, Y. Wang and C. A. Mirkin, *Nat. Nanotechnol.* 2007,

3, 145; D. V. Vezenov, A. Noy, L. F. Rozsnyai and C. M. Lieber, *J. Am. Chem. Soc.* 1997, **8**, 2006.
13 A. W. Peterson, R. J. Heaton and R. M. Georgiadis, *Nucleic Acids Res.* 2001, **24**, 5163.
14 P. Gong and R. Levicky, *Proc. Natl. Acad. Sci.* 2008, **14**, 5301; C. Fan, K. W. Plaxco and A. J. Heeger, *Proc. Natl. Acad. Sci.* 2003, **16**, 9134.
15 D. Wang, S. Gou and D. Axelrod, *Biophys. Chem.* 1992, **2**, 117; J. H. Monserud and D. K. Schwartz, *ACS Nano* 2014, **5**, 4488.
16 T. M. Herne and M. J. Tarlov, *J. Am. Chem. Soc.* 1997, **38**, 8916.
17 T. G. Drummond, M. G. Hill and J. K. Barton, *Nat. Biotechnol.* 2003, **10**, 1192; U. Rant, E. Pringsheim, W. Kaiser, K. Arinaga, J. Knezevic, M. Tornow, *et al. Nano Lett.* 2009, **4**, 1290; J. N. Murphy, A. K. H. Cheng, H. Z. Yu and D. Bizzotto, *J. Am. Chem. Soc.* 2009, **11**, 4042; Y. Chen, A. Nguyen, L. Niu and R. M. Corn, *Langmuir* 2009, **9**, 5054; L. M. Demers, D. S. Ginger, S. J. Park, Z. Li, S. W. Chung and C. A. Mirkin, *Science* 2002, **5574**, 1836.
18 E. A. Josephs and T. Ye, *ACS Nano* 2013, **4**, 3653; H. H. Cao, N. Nakatsuka, A. C. Serino, W. Liao, S. Cheunkar, H. Yang, *et al. ACS Nano* 2015, **11**, 11439; F. C. Macazo, R. L. Karpel and R. J. White, *Langmuir* 2015, **2**, 868; L.Yang, C. Zhang, H. Jiang, G. Li, J. Wang and E. Wang, *Anal. Chem.* 2014, **10**, 4657.
19 M. Liu, N. A. Amro and G. Liu, *Annu. Rev. Phys. Chem.* 2008, **59**, 367; G. Doni, M. D. N. Ngavouka, A. Barducci, P. Parisse, A. De Vita, G. Scoles, L. Casalis, G. M. Pavan, *Nanoscale* 2013, **20**, 9988.
20 M. Liu and G. Y. Liu, *Langmuir* 2005, **21**, 1972; E. Mirmomtaz, M. Castronovo, C. Grunwald, F. Bano, D. Scaini, A. A. Ensafi, *et al. Nano Lett.* 2008, **12**, 4134.
21 G. R. Abel, E. A. Josephs, N. Luong and T. Ye, *J. Am. Chem. Soc.* 2013, **17**, 6399.
22 S. Woo and P. W. Rothemund, *Nat. Comm.* 2014, **5**, 5610.
23 E. A. Josephs and T. Ye, *J. Am. Chem. Soc.* 2010, **30**, 10236.
24 G. R. Abel, B. H. Cao, J. E. Hein and T. Ye, *Chem. Commun.* 2014, **50**, 8131.
25 C. Rivetti, M. Guthold and C. Bustamante, *J. Mol. Biol.* 1996, **5**, 919.
26 H. G. Hansma and D. E. Laney, *Biophys. J.* 1996, **4**, 1933.
27 I. Rouzina and V. A. Bloomfield, *J. Phys. Chem.* 1996, **23**, 9977; N. Grønbech-Jensen, R. J. Mashl, R. F. Bruinsma and W. M. Gelbart, *Phys. Rev. Lett.* 1997, **12**, 2477.
28 S. H. Kang, M. R. Shortreed and E. S. Yeung, *Anal. Chem.* 2001, **6**, 1091.
29 E. A. Josephs and T. Ye, *J. Am. Chem. Soc.* 2012, **24**, 10021; E. A. Josephs and T. Ye, *Nano Lett.* 2012, **10**, 5255.
30 T. Kakiuchi, M. Iida, S.-i. Imabayashi and K. Niki, *Langmuir,* 2000, **16**, 5397.
31 J. Jing, J. Reed, J. Huang, X. Hu, V. Clarke, J. Edington, *et al. Proc. Natl. Acad. Sci.* 1998, **14**, 8046; H. Tanaka and T. Kawai, Nat. *Nanotechnol*. 2009, **8**, 518.
32 S. H. Sternberg, S. Redding, M. Jinek, E. C. Greene and J. A. Doudna, *Nature* 2014, **7490**, 62.
33 A. Bensimon, A. Simon, A. Chiffaudel, V. Croquette, F. Heslot and D. Bensimon, *Science* 1994, **5181**, 2096; T. Matsuoka, B. C. Kim, J. Huang, N. J. Douville, M. D. Thouless and S. Takayama, *Nano Lett.* 2012, **12**, 6480.
34 X. Sun, S. H. Ko, C. Zhang, A. E. Ribbe and C. Mao, *J. Am. Chem. Soc.* 2009, **37**, 13248; R. J. Kershner, L. D. Bozano, C. M. Micheel, A. M. Hung, A. R. Fornof, J. N. Cha, *et al. Nat. Nanotechnol.* 2009, **9**, 557; A. Aghebat Rafat, T. Pirzer, M. B. Scheible, A. Kostina and F. C. Simmel, *Angew. Chem. Int. Ed.* 2014, **29**, 7665.

